Acta Mech 210, 1–12 (2010)
DOI 10.1007/s00707-009-0191-2

Bhadraiah Vempati · Mahesh V. Panchagnula · Alparslan Öztekin · Sudhakar Neti

Combined buoyancy and viscous effects in liquid–liquid flows in a vertical pipe

Received: 13 November 2008 / Revised: 15 May 2009 / Published online: 21 June 2009

Abstract This paper presents experimental and numerical results of interfacial dynamics of liquid–liquid flows when an immiscible core liquid is introduced into a continuous liquid flow. The fully developed flow model predicts multiple solutions of the jet diameter over a range of dimensionless numbers: flow rate ratio, viscosity ratio, Bond and Capillary numbers. Experiments have been carried out using Polyethylene Glycol (PEG) and Canola oil to investigate the realizability of the three possible solutions predicted by the fully developed flow model. The measured values of inner fluid radii agree very well with the lower branch of the three branched solution while deviating from the top branch beyond a critical flow ratio value. This deviation is attributed to the fact that the flow develops a non-axisymmetric solution at this critical point. Computational fluid dynamics simulations have also been performed to examine the developing core annular flow and to compare the analytical solution results of liquid jet radius. The results predicted by numerical simulations agree very well with both the lower and upper branches of solution predicted by the analytical theory.

List of symbols

b	Fractional area occupied by the jet, $\frac{R_1}{R_2}$
f	Pressure gradient in axial direction, Pa/m
g	The magnitude of gravitational acceleration, ms^{-2}
P	Pressure of fluid
r	Radial co-ordinate direction
t	Subscript, t represents the partial derivative of variable with respect to t
$\mathbf{V}$	Velocity vector
z	Axial co-ordinate direction
$R(\theta, z, t)$	Radius of inner fluid with respect to θ, z, t
R_1	Fully developed radius of the inner fluid, m
R_2	Tube radius, m
R_i	Nozzle inner radius, m
R_o	Nozzle outer radius, m

B. Vempati · A. Öztekin · S. Neti
Department of Mechanical Engineering, Lehigh University, Bethlehem, PA 18015, USA

M. V. Panchagnula (✉)
Department of Mechanical Engineering, Tennessee Technological University, Cookeville, TN 38505, USA
E-mail: mvp@tntech.edu

B. Vempati
ADM Associates, Sacramento, CA, USA

L_1	Length of nozzle, m
L_2	Length of tube, m
W_i	Axial velocity of fluid phase i, m/s; $i = 1, 2$ for inner and outer fluid phases, respectively
V_i	Fully developed axial velocity of fluid phase i, m/s; $i = 1, 2$ for inner and outer fluid phases, respectively
P_i	Pressure of fluid phase i, Pa; $i = 1, 2$ for inner and outer fluid phases, respectively
Q_i	Flow rate of fluid phase i, m^3/s; $i = 1, 2$ for inner and outer fluid phases, respectively
Re_i	Reynolds number, $\frac{\rho_i \overline{W}_i R_2}{\mu_i}$; $i = 1, 2$ for inner and outer fluid phases, respectively
$\overline{\mathbf{U}}$	Base flow velocity vector
$\overline{W}_1$	Average velocity of injected phase, m/s; $\frac{Q_1}{\pi R_i^2}$
$\overline{W}_2$	Average velocity of continuous phase, m/s, $\frac{Q_2}{\pi R_2^2}$ (here, $R_o/R_2 \ll 1$)
Bo/Ca	Ratio of Bond and Capillary numbers, $\frac{\pi(\rho_2-\rho_1)gR_2^4}{\mu_2 Q_2}$
η	Ratio of inner and outer fluid viscosities, $\frac{\mu_1}{\mu_2}$
α	Volume fraction function
λ	Flow ratio of inner and outer fluids, $\frac{Q_1}{Q_2}$
κ	Curvature, m^{-1}
μ	Weighted average viscosity in the interface region, Pa s
ρ	Weighted average density in the interface region, kg/m^3
σ	Surface tension, N/m
θ	Angular co-ordinate direction
λ^*	Critical value of λ
η^*	Critical value of η
Bo/Ca*	Critical value of Bo/Ca
μ_i	Viscosity of fluid phase i, Pa s; $i = 1, 2$ for inner and outer fluid phases, respectively
ρ_i	Density of fluid phase i, kg/m^3; $i = 1, 2$ for inner and outer fluid phases, respectively

1 Introduction

Immiscible multifluid flows have been the subject of scientific research for over a century. These flows occur in a wide variety of industrial applications: dispersive flows [1], liquid extraction processes [2,3], core annular flows [4], and co-extrusion flows [5]. In most industrial applications, liquids are dispersed into droplets by injecting a liquid through a nozzle or an orifice into another continuous liquid. The injected liquid may drip or form a long jet at the nozzle depending upon the flow rate and properties of the injected liquid relative to the continuous liquid [6]. For the fluids and flow rates of interest here, the injected fluid forms a continuous jet at the end of the nozzle and is commonly referred to as core annular flows. As one example, these cases are pertinent to water lubricated oil flows (core annular flows) in which the less viscous water encapsulates the oil to reduce frictional losses.

The flow structure in such a two fluid system is highly complex owing to several physical phenomena that affect it. The flow structure in creeping immiscible liquid–liquid flows in the jetting regime is governed by viscous and gravitational forces. The core fluid manifests multiple steady state radii for a given flow condition, depending on the initial condition. The current study investigates the combined effect of gravitational and viscous forces on the choice of steady state core fluid jet radius. The results of this study will demonstrate the parameter set where multiple stable steady states are possible.

Because generalized stability analysis of multiphase flows is complicated, most stability studies are confined to perfect core annular flows (PCAF). Several researchers [7–10] have studied the stability of PCAF. They were able to predict the onset of snake and corkscrew waves on the PCAF from their theoretical analysis. These two types of waves correspond to the real parts of the azimuthal wave number being one with zero and non-zero imaginary parts, respectively. Bai et al. [7] performed an extensive experimental study of vertical oil–water core annular flows with the lighter fluid (oil) as the core fluid. They showed the presence of axisymmetric waves under upflow conditions and corkscrew waves under down flow condition. Hu and Patankar [9] studied the linear stability of CAF of water and oil. They predicted that the flow is most unstable to non-axisymmetric sinuous mode of disturbances ($n = 1$) when the oil core is small in radius in comparison with the pipe radius.

However, when the core of the radius approaches the radius of the pipe, axisymmetric disturbance mode is the most destabilizing. See the review article by Joseph et al. [11] for an overview of the research on the stability of core annular flows.

Recently, Kouris and Tsamopoulos [12,13] studied the non-linear dynamics of concentric flow of two immiscible fluids in a circular tube. They showed that saturated waves resembling the bamboo wave form will occur when the viscosity ratio (ratio of core and annulus phase fluids) is greater than unity [12]. This is in contrast to saw tooth wave forms that are observed when the viscosity ratio is equal to or less than unity [13]. Ooms and Poesio [14,15] studied the core annular flow in a horizontal tube with the heavier and more viscous fluid in the core portion of the tube. Their study focused on the interaction between buoyancy forces and other hydrodynamic forces and showed that the lubrication force counterbalances the buoyancy forces for the case when non-axisymmetric "snake" waves develop at the free surface. They also demonstrated that for large enough pressure gradients, a balance between buoyancy force and hydrodynamic force causes the development of eccentric core annular flows. Recently, Kang et al. [16] studied the buoyancy effects in water-oil flows in a vertical pipe using level set based simulations. Their simulations predicted the occurrence of bamboo waves similar to those observed by Bai et al. [7]. In the cases reported in the literature where vertical liquid–liquid flows were the subject of study, the injected fluid was lighter than the surrounding annular fluid. This causes the buoyancy to naturally form a stabilizing force. We herein present a study of cases, where that force is naturally *destabilizing*.

Most previous studies have investigated liquid–liquid flows when the heavier and more viscous fluid in the annulus of the tube, with the injected fluid being lighter than the core fluid. This configuration results in only one core radius solution for all flow conditions. We herein choose to investigate cases where the injected fluid is heavier and more viscous than the core fluid. This case is interesting as it could imply the possibility of multiple core radius solutions. Recently, Vempati et al. [17,18] studied the interfacial dynamics of liquid–liquid co-axial flows under such condition, where the injected phase liquid is introduced in the central portion of the annular continuous phase liquid while both fluids are in motion. They investigated the effect of flow rate ratio, viscosity ratio, Bond number, and Capillary number on the interface evolution of the liquid phases and injected liquid phase jet radius using FLUENT® software's [19] volume of fluid (VOF), continuous surface force (CSF) numerical scheme. The numerical simulations in [17] compared favorably with the experimental measurements of Kettering [20] as well as fully developed flow model results.

The current work presents results of a comprehensive experimental, numerical and theoretical investigation of the possibility of multiple steady states as a heavier inner fluid is introduced co-axially into the central portion of a pipe under vertical flow conditions. We demonstrate using the theoretical analysis that multiple axisymmetric steady states are possible and that the transition behavior between the multiple steady states involves hysteresis under certain parameter conditions. In addition, at the critical point, we show the existence of a new non-axisymmetric stable solution branch. The focus of this work is to identify these multiple solutions and the critical non-dimensional parameters where bifurcations in these solutions occur, using both theoretical and experimental techniques.

2 Experimental setup

Immiscible, liquid–liquid, co-current Poiseuille flows were investigated experimentally in vertical pipe geometry. The test fluids used in these experiments are dilute aqueous solution of Polyethylene Glycol (PEG) and Canola oil. The properties of the test fluids are given in Table 1. A schematic of the experimental setup is shown in Fig. 1.

PEG is introduced into Canola oil flowing in a vertical pipe (0.075 m diameter and 1.2 m in length) geometry through a nozzle (0.0254 m inside diameter and 0.102 m in length) as shown in Fig. 1. The Canola oil is introduced separately into the annular portion. The individual fluid flow rates are measured using two model GM002R2R41-4 positive displacement flow meters. Compressed air is used to drive the fluids through the

Table 1 Properties of the test fluids used in the experiments

Fluid properties	ρ, Density (kg/m^3)	μ, Viscosity (Pa s) at 21°C	σ, Interfacial tension of a PEG and Canola oil (N/m)
PEG solution	1,070	0.54	0.0177
Canola oil	900	0.0515	

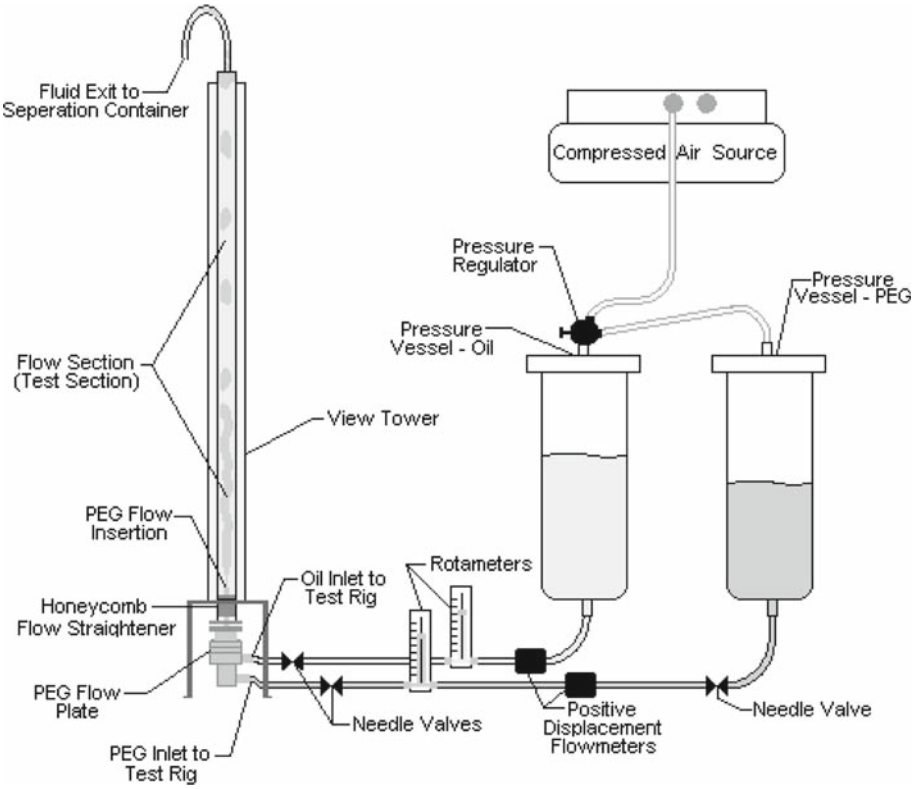

Fig. 1 Schematic of test rig

system. The fluids come into contact at the end of the nozzle introducing the PEG fluid. Images of the flow field were recorded with a video camera (Sony DCR-TRV250, Digital 8) at various PEG and Canola oil flow rates. The image analysis software SPOTLITE-16 [21] was then used to extract the information pertaining to the shape of the interfacial profiles from the individual video frames.

The inner and outer fluids are introduced concentrically through the nozzle and the annulus portion of the tube, respectively, at different velocities. The region immediately downstream of the nozzle is one where the two phases are not in equilibrium. If the injected phase momentum flux during this non-equilibrium stage is higher than that of the outer fluid, then the injected liquid phase will decelerate and its diameter will increase. If the injected fluid momentum flux is lower, the injected phase fluid core diameter will decrease as this fluid is accelerated. The jet subsequently reaches an asymptotic constant radius, indicating that the fully developed flow condition is reached. The fully developed flow condition is said to have been reached only if the jet radius remains unchanged over a long axial distance. This core fluid radius is measured and presented as a function of the various flow parameters. A more detailed description of the experimental configuration and test procedure is given in Kettering [20].

3 Governing equations and mathematical basis

The problem of immiscible liquid–liquid flows has been solved with FLUENT® using the VOF/CSF technique to track the fluid interface. In this method, a single momentum equation is solved for the pressure and velocity field in the multifluid domain.

The flow is assumed to be axisymmetric, incompressible, isothermal and laminar. Viscosity of the two phases and their relative interfacial tension are assumed to be constant throughout the flow domain. For this case, the governing equations are:

$$\nabla.\mathbf{V} = 0, \tag{1}$$

$$\rho\frac{\partial \mathbf{V}}{\partial t} + \rho\nabla\cdot(\mathbf{VV}) = -\nabla P + \nabla\cdot\mu\left[(\nabla\mathbf{V}) + (\nabla\mathbf{V})^T\right] + \rho g + \sigma\kappa\nabla\alpha. \tag{2}$$

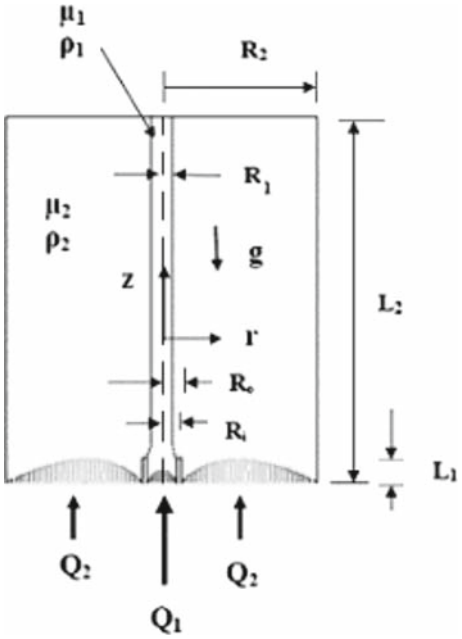

Fig. 2 Flow geometry used in the CFD simulations

The last term in Eq. (2) arises due to surface tension acting on the liquid–liquid interface and is treated as a body force [22]. The volume fraction α assumes values of unity and zero in the two fluids, respectively. α varies smoothly from zero to unity near the interface. This method provides a simple and economical way to track free surfaces in complicated multi-fluid flows with the help of a volume fraction function. The equation that governs the distribution of the volume fraction function, α, is:

$$\frac{\partial \alpha}{\partial t} + (\mathbf{V} \cdot \nabla)\alpha = 0 \tag{3}$$

The liquid properties, viz. density and viscosity, of the two fluids at the interface are estimated by a weighted averaged method:

$$\rho = \alpha\rho_2 + (1-\alpha)\rho_1, \quad \mu = \alpha\mu_2 + (1-\alpha)\mu_1. \tag{4}$$

The flow configuration employed in the present work is shown in Fig. 2. Two immiscible liquids are made to flow up a vertical tube of radius R_2. One fluid is introduced in the inner portion (center) of the pipe while the other fluid is introduced in the outer annulus portion of the tube. The interface between the two liquids is described by $r = R(\theta, z, t)$ where (r, θ, z) describe a cylindrical coordinate system as shown in Fig. 2. The inner phase fluid occupies the region $0 \leq r \leq R(\theta, z, t)$ while the outer phase fluid occupies the region $R(\theta, z, t) \leq r \leq R_2$. For the remainder of this paper, inner and outer phase fluids are labeled with subscript values $i = 1, 2$, respectively. The interfacial tension between the liquids, σ, is assumed to be constant. Gravity, g, is acting in the downward direction.

The coordinates z and r are measured in units of R_2 and velocity is measured in units of average inner fluid velocity, $\overline{W}_1 = Q_1/\pi R_1^2$. From a dimensional analysis, we find that the dimensionless numbers that govern the flow are the ratio of the Bond number, Bo, (which evaluates the relative influence of gravitational forces to the surface tension forces) to the Capillary number, Ca, (which measures the influence of viscous forces relative to the surface tension forces), the flow ratio, $\lambda = Q_1/Q_2$, and the viscosity ratio, $\eta = \mu_1/\mu_2$.

The boundary conditions imposed on the velocity field in polar coordinate system (r, z) are as follows:

At the inlet ($z = 0$), the injected phase and the continuous phase flows are considered to be fully developed. No slip and no penetration conditions are imposed at the inner and outer walls of the nozzle and at the surface of the tube. At the outlet ($z = L$), the pressure is maintained constant. Both fluids enter the flow field shown in Fig. 2 with fully developed velocity profiles. The domain is initially filled with the annular fluid. At time $t = 0$, the core fluid is injected into the domain with a parabolic velocity profile. Time resolved simulations are subsequently carried out until steady state is achieved. By this methodology, we allow the system to reach

any desired steady state from among a multitude of possible solutions. Details of numerical model including its numerical convergence are presented in Vempati et al. [17].

3.1 Perfect core annular flow: governing equations

The base flow is assumed to be a PCAF, where the conditions are:

$$\overline{\mathbf{U}} = (0, 0, V_i(r)), \quad i = 1, 2, \tag{5}$$

$$R(\theta, z, t) = R_1, \tag{6}$$

$$\text{at} \quad r = R_1, \quad P_1 - P_2 = \frac{\sigma}{R_1}. \tag{7}$$

The steady state, fully developed velocity profile for the flow in a pipe of a pair of immiscible fluids—one fluid in the core (fluid 1) and the other forming an annulus (fluid 2)—is well known [4] and is given by

$$V_1(r) = \frac{f - \rho_1 g}{4\mu_1}\left(R_1^2 - r^2\right) + \frac{f - \rho_2 g}{4\mu_2}\left(R_2^2 - R_1^2\right) - \frac{R_1^2(\rho_1 - \rho_2)g}{2\mu_2}\ln\left(\frac{R_2}{R_1}\right), \quad 0 \le r \le R_1, \tag{8}$$

$$V_2(r) = \frac{f - \rho_2 g}{4\mu_2}\left(R_2^2 - r^2\right) + \frac{R_1^2(\rho_1 - \rho_2)g}{2\mu_2}\ln\left(\frac{r}{R_2}\right), \quad R_1 \le r \le R_2, \tag{9}$$

where f is the pressure gradient in both phases and constant, $f = -\frac{\mathrm{d}P_1}{\mathrm{d}z} = -\frac{\mathrm{d}P_2}{\mathrm{d}z}$ (the pressure gradient, f in both phases has to be equal for the flow to remain perfectly core annular with a constant core radius).

The radius of the cylinder that the core fluid occupies is determined by the choice of Q_1 and Q_2. For a given pair of volumetric flow rates, Q_1 and Q_2, we calculate f for each fluid phase. By setting the pressure gradient in the two phases to be equal, we arrive at a non-linear equation that determines the core fluid radius. The resulting equation for the non-dimensional core fluid radius, $b = \frac{R_1}{R_2}$, in terms of λ, η, Bo and Ca is presented below:

$$\frac{\pi \mathrm{Bo}}{\mathrm{Ca}}\left(\begin{array}{l}\frac{b^6(1-b^2)}{4\eta} + b^4\left(1-b^2\right)^2\left[\frac{1}{2} + \frac{\ln(b)}{2} - \frac{1}{8\eta}\right] \\ \quad +(4b^6)\ln(b)\left[\frac{b^2}{8\eta} + \frac{1-b^2}{4}\right]\end{array}\right) + \frac{b^4}{\eta} + 2b^2(1-b^2) - \lambda(1-b^2)^2 = 0. \tag{10}$$

Here $\frac{\mathrm{Bo}}{\mathrm{Ca}} = \frac{\pi(\rho_2 - \rho_1)gR_2^4}{\mu_2 Q_2}$, $\lambda = \frac{Q_1}{Q_2}$ and Q_1, Q_2 are the volumetric flow rates of the core and annular fluids.

Equation (10) is a transcendental equation with potentially multiple roots for b in the range $0 < b < 1$ (the limits on b arise from the fact that the core fluid radius has to be positive and cannot exceed the tube radius). It is solved numerically to determine b for a set of non-dimensional parameters, viz. Bo/Ca, λ, and η. Depending on the parameter set, the equation has one, two or three solutions for b in the range $0 < b < 1$.

4 Results and discussion

Figure 3 is a plot of the fully developed jet radius versus λ at fixed values of Bo/Ca = 97.5, $Re_2 = 12$, and $\eta = 10.5$. The non-dimensional core fluid radius predicted by Eq. (10) and that obtained from axisymmetric computational fluid dynamics (CFD) simulations as well as experimentally measured values are plotted in Fig. 3 as a function of λ. The experimental and numerical simulations results are denoted by open triangles and circles, respectively, while the analytical solution results are shown by the solid and dotted lines. From Fig. 3, we can identify two critical flow ratio (λ) values of 0.017 and 0.023, marked as points B and A, respectively. For the values of λ between 0.017 and 0.023, we identify three possible steady state solutions whereas for the rest of the λ values (i.e., $\lambda < 0.017$ and $\lambda > 0.023$) only one solution exists. The critical points on the curve corresponding to $\lambda = 0.017$ and 0.023 are bifurcation points of the second kind, where the solution branch changes its stability characteristics from stable to unstable and vice versa. For this reason, the upper and lower solution branches present stable solutions while the middle branch is linearly unstable [23]. This system exhibits classical hysteresis behavior where the solution for Bo/Ca = 97.5, $Re_2 = 12$, and $\eta = 10.5$ and $\lambda < 0.023$ is presented by the lower branch. As λ increases, the solution follows the lower branch until the

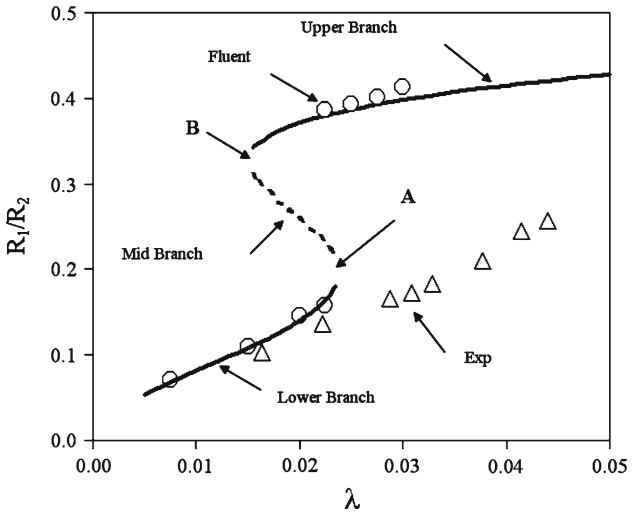

Fig. 3 Fully developed radius solutions of different λ at Bo/Ca = 97.5, $\eta = 10.5$ and $Re_2 = 12$

critical value of $\lambda = 0.023$ (A) is reached. At this point, a small increase in the value of λ causes the core fluid radius to increase to reach the solution indicated by the upper branch. As λ increases further, the solution for the core jet radius follows the upper branch. When λ is gradually reduced from a value of $\lambda > 0.023$, the solution for the core jet radius follows the upper branch until a second critical value of $\lambda = 0.017$ (B) is reached. At this point, further decrease in λ causes the solution to be dramatically decreased and reaches the solution predicted by the lower branch. Therefore, in the parameter regime $0.017 < \lambda < 0.023$, the value of the core jet radius depends on the direction in the parameter space from which the state is approached. Observations of this classical hysteretic behavior in this flow, validated by CFD and experimental measurements, are being presented for the first time.

The circles in Fig. 3 represent the core jet radius calculated from time resolved CFD simulations. As can be observed, the axisymmetric CFD results follow the lower and upper branches of the three-branched solution very well with a maximum deviation of 10%. The predicted hysteresis behavior described earlier was realized from these CFD simulations as well. This hysteretic behavior is similar to that observed in relaxation oscillations of the Duffing equation [24]. Therefore, as can be seen by comparing the solutions from Eq. (4) to the exact CFD solution, the dynamics and stability of the multiple steady state solutions can be studied by simply analyzing the characteristics of the roots of Eq. (10).

Figure 3 also presents experimentally measured values of the core fluid radius versus λ. As can be seen, the experimental measurements agree with the lower branch of the three-branched solution within an experimental uncertainty of 10% for $\lambda < 0.023$. As λ increases, the analytical solution predicts that at the critical value of $\lambda = 0.023$, the core radius would increase to match the upper solution branch. However, the experimental results for $\lambda > 0.023$ do not match the radius values predicted by the PCAF axisymmetric solutions (the upper branch) as well as the axisymmetric CFD simulations, but seem to follow a fourth solution branch. The deviation observed at the critical point A between the theoretical results and the experimental measurements is due to the development of a new non-axisymmetric solution branch that could not be discovered by the axisymmetric theoretical analysis and CFD simulations. This hypothesis is substantiated by the data in Fig. 4 as well as examples of the flow structures observed for $\lambda < 0.023$ and $\lambda > 0.023$ (see Fig. 5a, b, respectively).

Figure 4 is a plot of the non-dimensional core radius versus non-dimensional pressure gradient for the three solution branches in Fig. 3. The pressure gradient is a measure of the energy dissipation in the flow. As can be seen from this figure, the pressure gradient for the upper solution branch is much higher than that for the lower solution branch. This implies that the jump from the lower branch to the upper branch at the critical point A implies a high energy cost. In response to this energetically expensive proposition, the flow chooses a new non-axisymmetric solution branch which is potentially less dissipative. This choice of steady state, which is based on the minimal dissipation rate principle, has also been observed in other multiphase flow situations [25]. The principle of minimal dissipation rate is generally based on the constructal theory [26] which ascribes a motive of maximizing sustainability (minimizing energy consumption and therefore dissipation rate) to all finite sized systems. Similar conclusions on horizontal core annular flow were also recently reached by Ooms

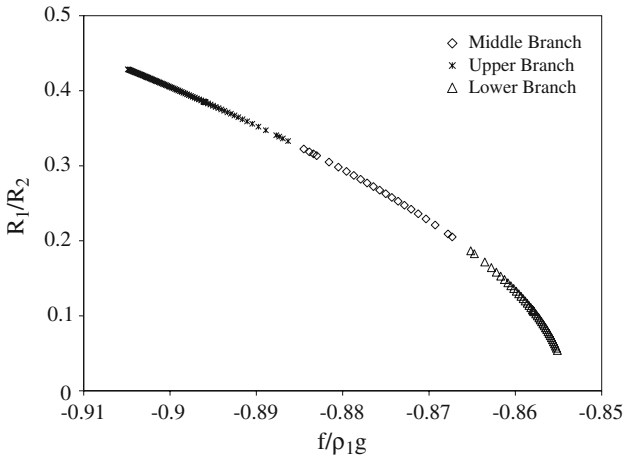

Fig. 4 Plot of the non-dimensional core radius versus non-dimensional pressure gradient

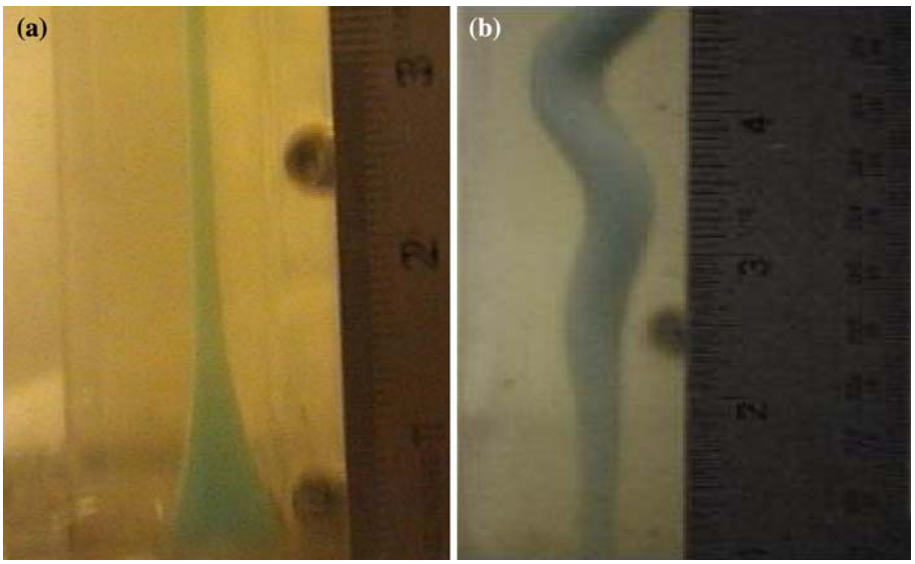

Fig. 5 Non-axisymmetric core flow picture at flow parameters: $\eta = 10.5$, $Re_1 = 0.7$, $Re_2 = 12$, and Bo/Ca = 97.5

and Poesio [14]. This solution branch was not discovered in the previous theoretical and CFD analyses owing to the fact that axisymmetry was imposed.

Experimental evidence of the development of this non-axisymmetric solution is provided in Fig. 5. Figure 5a was obtained at $\lambda = 0.015$ and Fig. 5b at $\lambda = 0.05$ for $\eta = 10.5$, $Re_1 = 0.7$, $Re_2 = 12$, Bo/Ca = 97.5. It can be observed from these images as well as from a temporal analysis of the video sequence that the flow remained axisymmetric for all $\lambda < 0.023$. However for $\lambda > 0.023$, the jet was observed to precess and developed a clear non-axisymmetric nature. This flow structure has been described as "corkscrew waves" by Bai et al. [7] and Renardy [10] An example of such a non-axisymmetric core flow is presented in Fig. 5b at $\lambda = 0.05$ (>0.023). It may be noted that the images in Fig. 5 are obtained for a region close to the injection region (the development region). A complete transient three dimensional CFD simulation with the free surface resolved could potentially discover this solution branch but is beyond the scope of the current paper.

Equation (10) indicates that the non-dimensional core radius is a function of three parameters, Bo/Ca, λ and η. For each set of Bo/Ca and η values, lower and upper critical bounds for the values of λ (critical points) can be established to determine the range where one, two or three steady state solutions exist. Figure 6 presents the upper and lower critical bounds of Bo/Ca as a function of flow ratio of liquids (λ) for $\eta = 1.0$, 10.5, and 21. For a given value of λ, three different solutions of fully developed radius are possible if the value of Bo/Ca ratio lies in the region between the upper and lower critical bound curves. For these parameter values, the

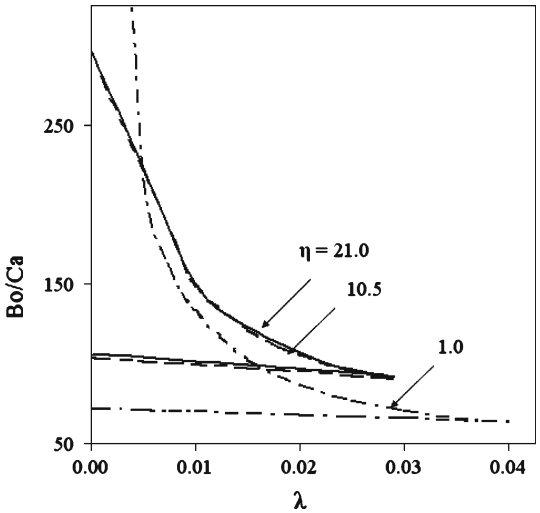

Fig. 6 Critical Bo/Ca numbers for different λ at Bo/Ca = 97.5 and $Re_2 = 12$

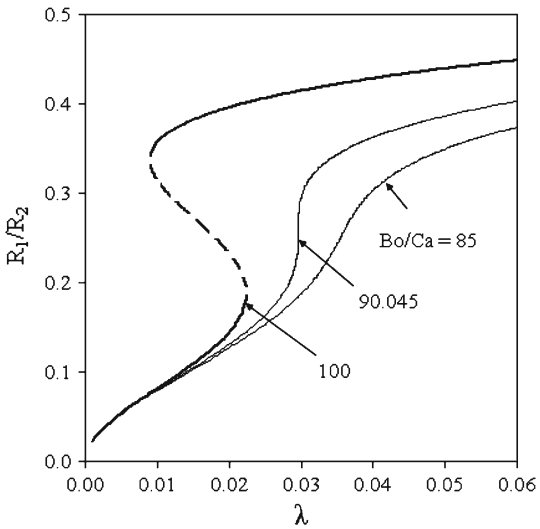

Fig. 7 Fully developed radius solutions versus λ for $\eta = 10.5$ and $Re_2 = 12$

hysteretic behavior described earlier is observed. When Bo/Ca takes on a value outside this region, only one steady state solution exists and the steady state behavior is monotonic and non-hysteretic. It is further evident from Fig. 6 that the upper and lower critical bounds for viscosity ratios 10.5 and 21 are almost identical, while those for $\eta = 1$ are significantly different. It can therefore be inferred that an asymptotic trend in the steady state behavior can be realized for large values of η, when the core fluid is significantly more viscous than the outer fluid. This case is of particular interest to oil pipeline lubrication flows [4] and will be revisited later. Finally, the upper and lower critical bounding curves in Fig. 6 meet at a point. This point represents a singular point bifurcation in the parameter space [27]. This point, λ^*, represents a degenerate case and corresponds to where $\frac{d\lambda}{db} = \frac{d^2\lambda}{db^2} = 0$ for a constant Bo/Ca and η.

Figure 7 is a plot of the non-dimensional radius of core fluid versus λ for $\eta = 10.5$ and for three values of Bo/Ca = 85, 90.045 and 100. It is observed for Bo/Ca = 85 that there is only one solution branch, whereas for Bo/Ca = 100 three solution branches are observed. In addition, Fig. 7 shows a singular point bifurcation for a critical value of $\lambda^* = 0.0296$ for $\eta^* = 10.5$ and Bo/Ca* = 90.045. This point is important in that for values of λ greater than this critical flow rate ratio, the flow remains axisymmetric. Figure 8 is a plot similar to Fig. 7, of the non-dimensional core fluid radius versus η for Bo/Ca = 90.045 and for varying λ. One solution

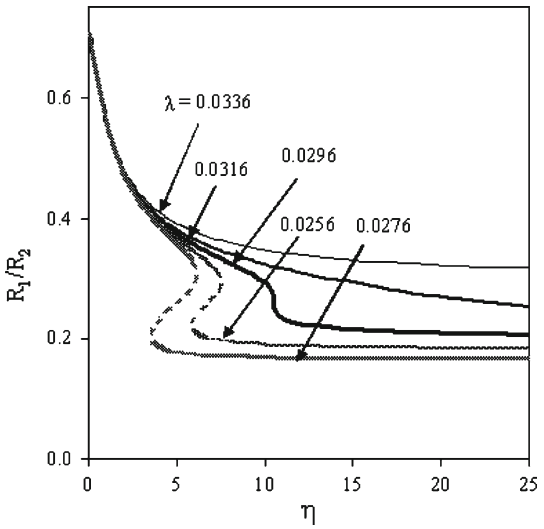

Fig. 8 Non-dimensional core radius versus η for sub-critical, critical and supercritical values of λ for Bo/Ca = 90.045

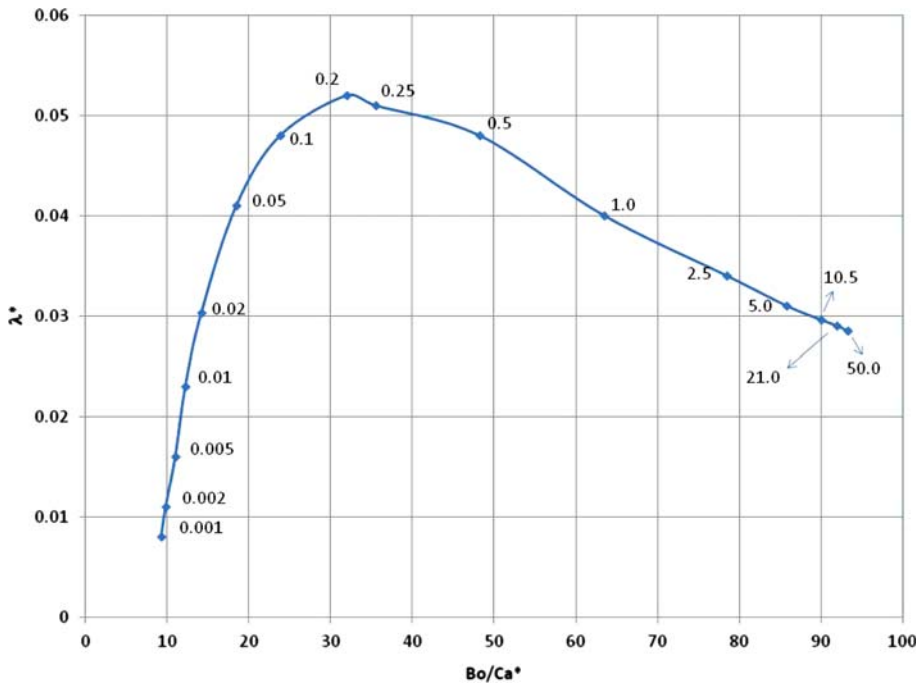

Fig. 9 Plot of critical value of λ versus critical value of Bo/Ca. The data labels indicate critical value of $\eta(\eta^*)$

exists for $\lambda > 0.0296$ and three solutions exist when $\lambda < 0.0296$. For $\lambda^* = 0.0296$ and Bo/Ca$^* = 90.045$, $\eta^* = 10.5$ again, only one solution exists but is a double root of Eq. (10).

For each value of Bo/Ca and η, a value of λ can be identified which represents a singular bifurcation point. This point, λ^*, represents the critical value which separates the regions of hysteretic from monotonic behavior. Figure 9 is a plot of this critical value λ^* versus Bo/Ca* for various values of η^*, which are shown as data labels next to the data points. Two features can be observed from this figure. For low values of η^*, λ^* initially increases and then decreases with increasing Bo/Ca*. For large values of η^*, the values of λ^* and Bo/Ca* reach asymptotic values of 0.0296 and 95, respectively. Large values of η^* are found in cases involving oil pipeline lubrication. When Bo/Ca* is 95, the critical value of λ^* determines the minimum flow rate of the lubricating fluid that is needed in order to maintain a stable core annular flow under vertical flow conditions and ensure perfect lubrication.

5 Conclusions

Fully developed (PCAF) axisymmetric flows of two immiscible liquids were studied in the context of bifurcations in the steady state behavior. These flows were studied using CFD simulations and fully developed flow theory (herein referred to as the analytical solution). The analytical solution predicted that the fully developed radius solutions of PCAF follow three branches, i.e., three possible core jet flow diameters, indicating two bifurcation points of the second kind. Experimental results agree very well with the lower branch (smallest possible core jet flow radii) of three branched axisymmetric solution within 10% of the predicted value. For flow rate ratio $\lambda > 0.023$ experiments do not indicate the presence of other axisymmetric solution branches. Numerical simulations using CFD with forced axisymmetric flow conditions agree very well with the lower (smallest radii) and upper branches (largest radii) of PCAF results. The hysteretic effect in these flows is also well captured by the CFD simulation. The core diameter jumps from the lower to the upper branch and vice versa at the two different bifurcation points in the solution space. Experiments performed with PEG-Canola oil suggest that the flow departs from purely axisymmetric flow conditions for the values of λ above the first bifurcation point. At this point, the flow is observed to develop a non-axisymmetric nature. Finally, the degenerate critical value which determines the onset of hysteresis and the non-axisymmetric nature is observed to take on an asymptotic value for large viscosity ratios. This conclusion would be useful in determining the critical flowrate ratio needed to maintain a stable core annular flow.

Acknowledgments Helpful discussions with Prof. Amalendu Mukherjee as well as the independent suggestions from reviewer #1 are gratefully acknowledged. These conversations helped shape the minimal dissipation rate theory arguments in this paper. Finally, the financial support of the Department of Energy, EERE program was partially responsible for the conduct of this research.

References

1. Meister, B.J.: The formation and stability of jets in immiscible liquid systems. Ph.D. Dissertation, Cornell University, Ithaca, New York (1966)
2. Treybal, R.E.: Liquid Extraction, 2nd edn. McGraw-Hill, New York (1963)
3. Jeffreys, G.: Review of the design of liquid extraction equipment. Chem. Ind. **6**, 181 (1987)
4. Joseph, D.D., Renardy, Y.: Fundamentals of Two-Fluid Dynamics. Springer, New York (1993)
5. Mavridis, H., Hrymark, A.N., Vlachopoulos, J.: Finite element simulation of stratified multiphase flows. AIChE J. **33**, 410 (1987)
6. Meister, B.J., Sheele, G.F.: Drop formation from cylindrical jets in immiscible liquid systems. AIChE J. **15**, 700 (1969)
7. Bai, R., Chen, K., Joseph, D.D.: Lubricated pipelining: stability of core annular flow. Part 5. Experiments and comparison with theory. J. Fluid Mech. **240**, 97–132 (1992)
8. Boomkamp, P.A.M., Miesen, P.A.M.: Non-axisymmetric waves in a core annular flow with a small viscosity Ratio. Phys. Fluids A **4**(8), 1627–1636 (1992)
9. Hu, H.H., Patankar, N.: Non-axisymmetric instability of core annular flow. J. Fluid Mech. **290**, 213–234 (1995)
10. Renardy, Y.: Snakes and corkscrews in core annular down-flow of two fluids. J. Fluid Mech. **340**, 297–317 (1997)
11. Joseph, D.D., Bai, R., Chen, K.P., Renardy, Y.Y.: Core annular flows. Ann. Rev. Fluid Mech. **29**, 65–90 (1997)
12. Kouris, Ch., Tsamopoulos, J.: Dynamics of axisymmetric core-annular flow in a straight tube: I. The more viscous fluid in the core, bamboo waves. Phys. Fluids **13**, 841–858 (2001)
13. Kouris, Ch., Tsamopoulos, J.: Dynamics of axisymmetric core annular flow II. The less viscous fluid in the core, saw tooth waves. Phys. Fluids **14**, 1011–1029 (2002)
14. Ooms, G., Poesio, P.: Stationary core annular flow through a horizontal pipe. Phys. Rev. **68**(6): Art No. 066301 Part 2 DEC 2003
15. Ooms, G., Vuik, C., Poesio, P.: Core annular flow through a horizontal pipe: hydrodynamic counterbalancing of buoyancy force on core. Phys. Fluids **19**, 092103 (2007)
16. Kang, M., Shim, H., Osher, S.: Level set based simulations of two-phase oil–water flows in pipes. J. Sci. Comput. **31**(1/2), 153–184 (2007)
17. Vempati, B., Panchagnula, M.V., Oztekin, A., Neti, S.: Numerical investigation of liquid–liquid co-axial flows. J. Fluids Eng. **129**, 713–719 (2007)
18. Vempati, B., Panchagnula, M.V., Oztekin, A., Neti, S.: Flow regimes of newtonian fluids in vertical co-axial flows. IMECE 2006-14111
19. FLUENT® User Guide. Lebanon, NH (2003)
20. Kettering, C.: Fluid dynamics of two immiscible liquids in a circular geometry. MSME Thesis, Lehigh University (2005)
21. Spotlight-16 Image Analysis Software, NASA Glenn Research Center Product, Cleveland, Ohio
22. Brackbill, J.U., Kothe, D.B., Zemach, C.: A continuum method for modeling surface tension. J. Comput. Phys. **100**, 335 (1992)
23. Minorsky, N.: Nonlinear Oscillations. Van Nostrand Press, London (1962)
24. Stoker, J.J.: Nonlinear Vibrations in Mechanical and Electrical Systems. Wiley Interscience, New York (1992)

25. Poesio, P., Beretta, G.P.: Minimal dissipation rate approach to correlate phase inversion data. Int. J. Multiph. Flows **34**(7), 684–689 (2008)
26. Bejan, A., Lorente, S.: Design with Constructal Theory. Wiley, New York (2008)
27. Iooss, G., Joseph, D.D.: Elementary Stability and Bifurcation Theory. Springer, Berlin (1989)